Plasma Chemistry and Plasma Processing (2024) 44:47–64
https://doi.org/10.1007/s11090-023-10416-w

ORIGINAL PAPER

Impact of Pressure and Hydrogen Dilution on the Kinetics of Methane Decomposition in AC-Excited, High Pressure Plasmas

Norleakvisoth Lim[1] · Yu Wu[1] · Michael J. Gordon[1]

Received: 2 August 2023 / Accepted: 11 October 2023 / Published online: 31 October 2023

Abstract
The kinetics of methane decomposition in low frequency (60 Hz) AC arc plasmas was investigated using on-line mass spectrometry and optical emission spectroscopy (OES) in a batch reactor configuration at pressures up to 3 bar absolute. Plasma conversion of CH_4 results largely from thermal dissociation and was seen to follow first-order kinetics up to high conversions (> 90%) without observing any rate impedance from reverse hydrocracking. H– and C-atom selectivities for H_2, C_2H_2, and C_2H_4 were 78% (1.56 mol H_2/mol CH_4 reacted), 36% (0.18 mol C_2H_2/mol CH_4), and 30% (0.15 mol C_2H_4/mol CH_4), respectively, at 3 bar. In other experiments, H_2 diluent concentration played an important role in CH_4 dissociation and final product distributions; H abstraction reactions increased the rate of CH_4 decomposition at low H_2 ($y_{H2} < 0.6$) while high H_2 ($y_{H2} > 0.6$) impeded CH_4 decomposition due to hydrocracking of C_2 products. The rate of CH_4 dissociation was seen to increase with pressure, up to 0.11 mol/m^3/s, and the specific energy requirement (SER) decreased with pressure to 365 kJ/mol CH_4 at 3 bar. The latter suggests that even higher operating pressures may improve the efficiency of plasma conversion of CH_4, and ultimately that plasma pyrolysis may be a viable and energy efficient route to clean (turquoise) H_2 and further implementation of chemical process electrification.

Keywords Plasma pyrolysis · Methane conversion · Hydrogen · Kinetics · High pressure

Introduction

The transition from fossil fuels to more sustainable energy sources has become a focus to combat climate change and achieve a sustainable and low carbon economy. Hydrogen, as an energy carrier, has been promoted as a promising solution to transitioning away from CO_2-emitting fuels. H_2 is an attractive energy carrier that can be derived from fossil fuels such as natural gas, with minimal to no CO_2 emission in the process, provided that some of the H_2 produced is used to power the conversion. Unfortunately, 95% of industrially

✉ Michael J. Gordon
gordon@ucsb.edu

[1] Department of Chemical Engineering, University of California, Santa Barbara, CA 93106, US

produced H_2 is via steam methane reforming (SMR), Eq. 1, which emits 9–12 kg of CO_2 per kg of H_2 produced [1, 2]. Hydrogen can also be produced through water electrolysis, Eq. 2, but the process is energetically expensive as it requires more energy for H_2 production than the energy yielded from the H_2 product itself. Methane pyrolysis however, Eq. 3, has recently regained interest due to its potential for net zero CO_2 emission, while theoretically requiring significantly lower energy compared to water hydrolysis and SMR [2].

$$CH_4 + 2H_2O(l) \rightarrow CO_2 + 4H_2 \qquad \Delta H^\circ = 63\text{kJ/mol}_{H_2} \tag{1}$$

$$H_2O(l) \rightarrow H_2 + \frac{1}{2}O_2 \qquad \Delta H^\circ = 286\text{kJ/mol}_{H_2} \tag{2}$$

$$CH_4 \rightarrow C(s) + 2H_2 \qquad \Delta H^\circ = 37\text{kJ/mol}_{H_2} \tag{3}$$

To be economically competitive with SMR, the reaction rates and energy efficiency of methane pyrolysis must be investigated and optimized. The (thermal) dissociation of CH_4 requires high operating temperature due to high C–H bond energy, 438.8 kJ/mol [3]. Moreover, conversion of CH_4 is significantly limited by a kinetic 'pseudo-equilibrium' at low temperature (< 1500 K) due to hydrocracking of products back to CH_4 [4]. This kinetic limitation is further exacerbated by increasing pressure [5], which is usually mandated to obtain industrially relevant reaction rates and throughput. The carbon product also causes collateral issues such as coking and catalyst poisoning, whose removal results in additional CO_2 emissions. However, plasma–based conversion of methane to hydrogen and carbon (as well as other hydrocarbons) is an attractive process due to a plasma's ability to generate non-thermal reactive species, improve conversion and utilize renewable energy resources easily.

Plasmas can be categorized as non-thermal, where electrons and ions/neutrals are not in equilibrium (high energy electrons and low temperature ions and neutrals), or thermal, where all species are in thermal equilibrium and gas temperatures are high. Both thermal and non-thermal plasmas have been extensively studied for the conversion of hydrocarbons, mainly CH_4 to H_2, high-valued carbon and/or higher hydrocarbons. In general, non-thermal plasmas such as dielectric barrier discharges (DBD), have lower conversion and higher selectivities for C_2H_6 and C_3–C_5 hydrocarbons [6–8]. Other plasmas that may transition between thermal and non-thermal states, such as pulsed discharges, microwave (MW) plasmas, and gliding arc discharges, tend to have higher conversion and higher selectivities for C_2 hydrocarbons and H_2 [6, 7, 9–15]. It should be noted that MW plasmas can achieve > 90% conversion below atmospheric pressure; however, throughput is low due to the low pressures involved. In addition, thermal plasma conversion of CH_4, using high current (> 1 A) DC/AC thermal arcs, has shown high conversion and demonstrated commercial viability for the production of carbon black and acetylene [16–19]. In particular, Monolith utilized a three-phase AC plasma jet/arc to convert CH_4 to high-valued carbon and hydrogen and achieved a specific energy requirement (SER) of 360 kJ/mol CH_4. They reported conversions higher than 95%, with 95% carbon and 99% H_2 yields [20]. Similarly, Polak and co-workers have shown up to 86% conversion, and 88.4% selectivity for C_2H_2, with a reported SER of 362 kJ/mol CH_4 using a DC plasma jet [18].

The specific energy required to dissociate CH_4 in plasmas can vary widely depending on the type of discharge, gas feed conditions, power input and discharge volume. Understanding the mechanism and kinetics behind the dissociation of CH_4 in thermal and non-thermal plasmas is therefore a crucial step to evaluating the efficacy of plasma conversion of methane and other hydrocarbons to H_2 and valuable products. Conventional kinetics

measurements using integral and/or differential flow reactors are not practical for plasma-based reactions. These measurements generally assume homogeneous reactivity throughout the reactor, which may not be true in the case of plasma. Furthermore, Kado et al. noted that not all gases flow through the discharge region in their reactor configuration [7]. This leads to lower conversion and can further complicate kinetics measurements.

In the present work, we investigate the kinetics, product distribution and SER of CH_4 dissociation using a low current AC arc discharge in a batch reactor configuration. The impact of pressure on the overall reaction rate and SER were examined from 0.5 to 3.0 bar absolute at different electrode gaps. In addition, the influence of H_2 partial pressure on the dissociation of CH_4 and C_2H_4 were investigated. The product distributions under different gas conditions are examined and the dominant reaction pathways are summarized. The carbon products were also evaluated using Raman spectroscopy, CH analysis, and microscopy.

Experimental Methodology

Reactor Design

Experiments were conducted in a batch reactor as shown in Fig. 1. The reactor body was constructed out of a stainless-steel cube with an opening of 64 mm internal diameter on each side. The total reactor volume was 923 mL. The electrode configuration consisted of a high voltage (HV) thoriated tungsten tip electrode and a stainless-steel plate ground electrode. The ground electrode was attached to a stepper motor that rotated at 0.5 Hz to break conductive carbon bridges that may form between the electrodes during the discharge. A fan was placed inside the reactor to induce circulation and ensure the reactor was well-mixed.

Plasma Source and Characterization

A 140 V variable transformer was used to supply power to a nominally 18 kV, neon light step-up transformer (Jefferson Transformer No. 721–111), which provided high voltage 60 Hz AC to the electrode. A series of 1500 Ω resistors were placed in series with the drive electrode to limit the current flow and protect the transformer. The voltage and current

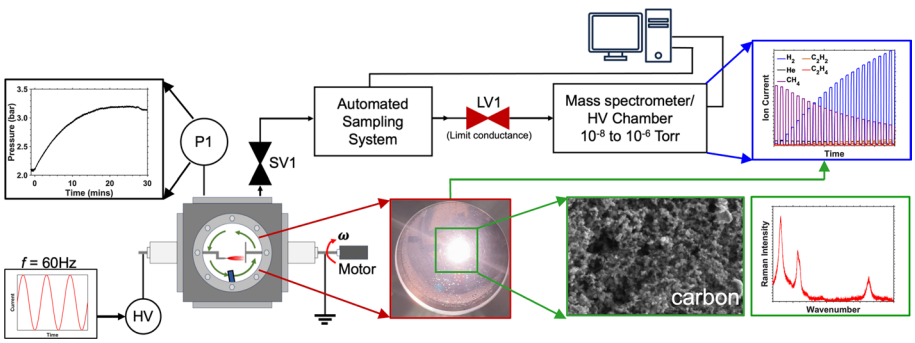

Fig. 1 Schematic of plasma batch reactor and on-line mass spectrometry measurement. SV1, LV1, and P1 denote sampling solenoid valve, limited conductance valve, and pressure transducer, respectively

were measured using a Tektronix P6015 high voltage probe and a Pearson 411 current transformer (Regowski coil). Thorlabs PDA 36A and APD430A Si photodetectors were used to measure optical emission transients. The probes and detectors were connected to an oscilloscope (Tektronix TDS 2004B) for data acquisition. Optical emission spectra were measured using an Ocean Optics USB 4000 spectrometer and the spectral intensity was corrected using an Ocean Optics Cal-2000 calibration light source as a reference.

Experimental Conditions and Gas Analyses

All experiments were carried out with 10 mol% helium gas as an internal reference unless specified otherwise. To compare the kinetics of methane conversion with different gas compositions and pressure, all experiments were carried out at the same root mean squared current (37 mA). Gas composition was analyzed through on-line mass spectrometry with Balzers QMS 200 and SRS RGA 300 mass spectrometers using a custom-built automated sampling system. During each experiment, a small volume of gas was extracted from the reactor and expanded into a sampling chamber at 6–7 Torr every 30 s. The sample gas was then leaked through a variable leak valve into a high vacuum (HV) chamber and analyzed by mass spectrometry. Supporting information S1 discusses the influence of this sampling methodology on the reaction kinetics measurement. C– and H-atom based product selectivities (S_i) are defined in Eqs. 4–6. A pressure transducer (Omega PX319–1KG5V) was used to monitor the reactor pressure throughout experiments.

$$S_{C_xH_y} = \frac{\text{moles of carbon in } C_xH_y \text{ produced}}{\text{moles of carbon in } CH_4 \text{ reacted}} \bullet 100\% = \frac{x \cdot n_{C_xH_y}(t)}{n_{CH_4}(t=0) - n_{CH_4}(t)} \bullet 100\% \tag{4}$$

$$S_C = \frac{\text{moles of carbon in solid carbon}}{\text{moles of carbon in } CH_4 \text{ reacted}} \bullet 100\% = 100\% - S_{C_2H_2} - S_{C_2H_4} \tag{5}$$

$$S_{H_2} = \frac{\text{moles of hydrogen in } H_2 \text{ produced}}{\text{moles of hydrogen in } CH_4 \text{ reacted}} \bullet 100\% = \frac{1}{2} \bullet \frac{n_{H_2}(t)}{n_{CH_4}(t=0) - n_{CH_4}(t)} \bullet 100\% \tag{6}$$

Here, S_i, $n_i(t)$ are selectivity of species i and moles of species i at time t, respectively.

Solid Carbon Analyses

The carbon product was examined using SEM (Thermo Fisher Scientific Apreo C at 5 kV/0.1 nA), CH analysis, and Raman (Horiba Jobin Yvon T64000 spectrometer with 647 nm excitation).

Results and Discussion

Optical and Electrical Characteristics of AC Arc Discharge

The current and voltage waveforms of the AC arc plasma demonstrate two distinct discharge regimes as shown in Fig. 2. The first regime constitutes initial breakdown of the

gas where an unstable intermittent arc or spark discharge occurs. This can be identified by a significant rise in voltage until the field intensity reaches the breakdown threshold, after which there is a sharp drop in voltage, followed by an increase in current flow as shown in Fig. 2b. The optical emission transient of the discharge corresponds to the current trace with pulse widths ranging from 500 ns to roughly 800 ns. The number of intermittent arcs tends to increase with pressure. The second discharge regime is characterized by a continuous and stable arc; the discharge voltage decreases as current increases due to increase in charge carriers and decrease in the plasma impedance.

A sequence of methane plasma images at different times is shown in Figs. 3a–d. As the arc discharge progresses, carbon is deposited on both the high voltage and ground electrodes, which effectively decreases the discharge gap. Over time, the deposited carbon can grow and form a conductive bridge between the electrodes, leading to a short circuit and extinguishing the arc discharge entirely within 20–30 s. To address this problem and extend the duration of each experiment, the ground electrode was attached to a motor, rotating at 0.5 Hz. A wedge was also placed on the ground electrode that removes carbon off the high voltage electrode. As a result, the discharge gap fluctuates periodically during the experiment due to carbon deposition and this mechanical carbon removal mechanism. The reported electrode gap length in this work is defined as the initial distance between the high voltage electrode and the ground plate electrode without considering carbon deposits. Figure 3e shows optical emission intensity, current and voltage transients during an arc discharge in CH_4. In contrast to the pure He discharge case (Fig. 2a), the optical emission from the CH_4 discharge fluctuates between each cycle. This demonstrates that the discharge volume fluctuates throughout the discharge process, which is attributed to carbon deposition on the electrode and changes in fluid dynamics resulting from gas expansion and reactions within the plasma.

The optical emission spectrum from CH_4 plasma is dominated by blackbody emission from soot particles as shown in Fig. 3f. An approximation based on the blackbody emission indicates that the plasma temperature is > 3000 K. Formation of diatomic carbon (C_2) is also observed based on its primary (Swan band) emission lines around 516 nm ($v = 0$), which suggests that some CH_4 likely dissociates into atomic carbon and hydrogen. As H_2 composition increases, less soot particles are formed as suggested by the decrease in

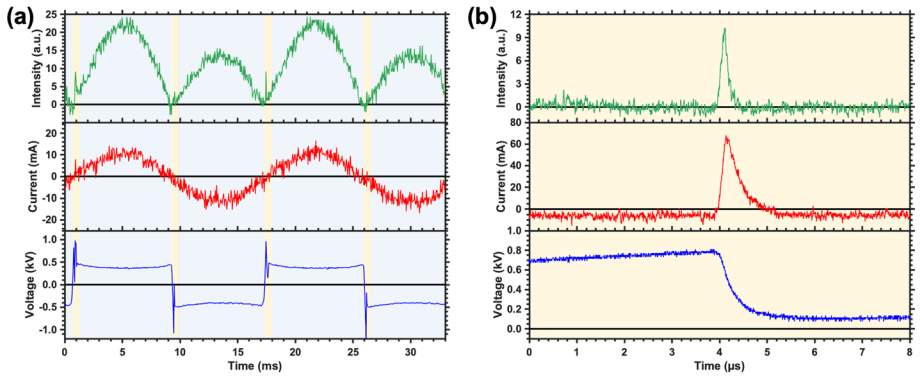

Fig. 2 Optical emission intensity, current and voltage characteristics of a He discharge at 1 bar. **a** Transient characteristics over two AC cycles, which show intermittent (yellow shaded) and stable (blue shaded) arc regimes. Panel **b** focuses on transient characteristics during the intermittent discharge (yellow shaded regions in panel (**a**)). The optical emission intensity is the integral over the visible spectrum (Color figure online)

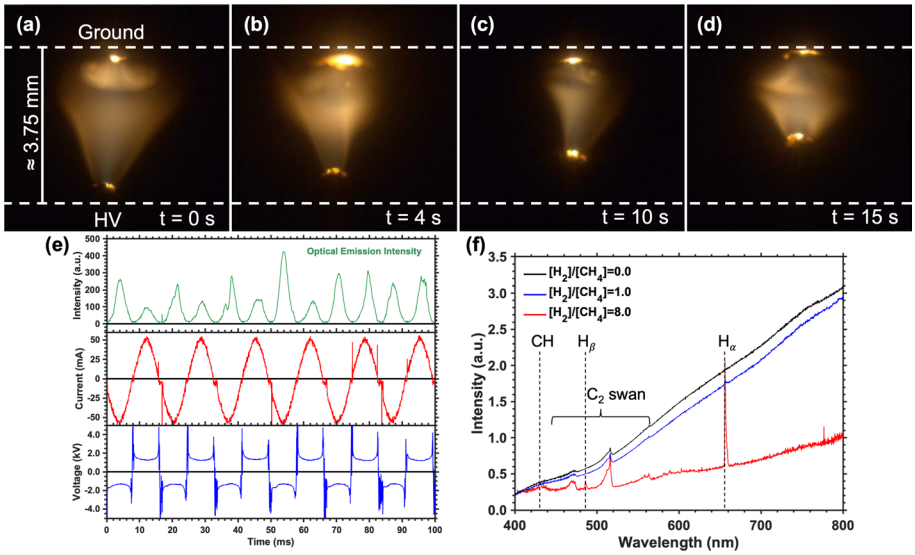

Fig. 3 **a**–**d** Temporal evolution of a typical (10% He/90% CH_4) discharge at 2 bar. Time series images show carbon growth on the high voltage (HV) electrode tip. **e** Optical emission intensity, current and voltage corresponding to the discharge in panels (**a**–**d**). **f** Optical emission spectra of different CH_4 and H_2 mixtures (with 10% He) as noted in the figure

blackbody emission intensity, which reveals H_α, H_β, and CH primary ro-vibrational lines at 656 nm, 486 nm, and 431 nm, respectively.

Plasma-Based Decomposition of Methane in a Batch Reactor

Figure 4 shows the pressure trace and gas composition during a discharge in a 10:90 mol% He:CH_4 mixture at 2 bar initial pressure. As the reaction progresses, there is a rise in the reactor pressure corresponding to an increase in the overall gas moles. On-line mass spectrometry measurements in Fig. 4b show increases in the C_2H_4, C_2H_2, and H_2 mole fractions as CH_4 is decomposing. No mass peak associated with C_2H_6 was detected. The He mole fraction appears to be decreasing because the total number of gas moles in the reactor is increasing, while the amount of helium remains the same. It is important to note that mass spectrometry measurement can only determine the mole fraction of gas species in a batch reactor, but it cannot provide information regarding the concentration. As such, we specifically used He as an internal reference to determine the actual concentrations of CH_4 and major products (further information in supporting information S2). Figure 4c shows the decay of methane concentration normalized to its initial concentration during the discharge.

There are two main pathways for the initial dissociation of methane in a discharge. In a non-thermal plasma with high energy electrons and high enough electron density, methane is more likely to decompose through electron impact dissociation, Eq. 7, which has an energy threshold of 9 eV [11]. Further dissociation into methylene, methylidyne, and carbon atom is also possible if the density of energetic electrons is high enough. As the electron energy decreases (<10 eV), the cross-sections for electron impact dissociation reactions in CH_4

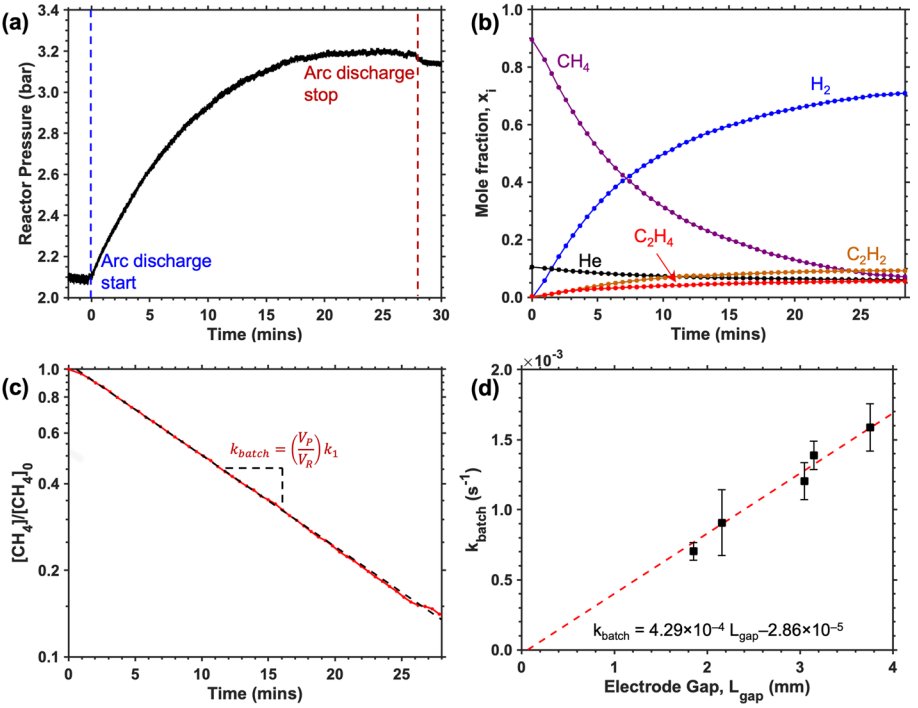

Fig. 4 Pressure and gas analyses of (10% He/90% CH_4) discharge at 2 bar and 2.8 mm electrode gap length. **a** Reactor pressure increases as a function of time during the discharge. **b** Time evolution of CH_4, He and major gaseous product mole fractions during the reaction. **c** Concentration of CH_4 decays exponentially as a function of time, which follows a first-order rate of reaction. **d** Reaction rate constant increases linearly with electrode gap

plasma decrease, while the cross sections for vibrational excitation through electron impact increase [21]. In this scenario, most of the energy transferred from electron collisions goes into exciting CH_4 molecules to a higher vibrational state, $CH_4(v)$. In nanosecond pulsed discharges, the internal vibrational energy of CH_4 can exceed the required bond dissociation energy, 4.5 eV, which leads to dissociation into CH_3 radicals, shown in Eq. 8 [12]. As for discharges with longer pulse duration, the vibrational excited states are quenched and the vibrational temperature of CH_4 molecules equilibrate with their rotational and translational temperatures. Then, the dissociation of CH_4 occurs similarly to a thermal process.

$$e + CH_4 \rightarrow CH_3 + H \tag{7}$$

$$e + CH_4 \rightarrow CH_4(v) \rightarrow CH_3 + H \tag{8}$$

In either case, the rate of methane dissociation can be modeled as pseudo first-order in a batch reactor as shown in the following:

$$\frac{d[CH_4]}{dt} = -k_1[CH_4] \tag{9}$$

where $[CH_4]$ and k_1 are CH_4 concentration and reaction rate constant, respectively. This model neglects the contribution from reverse reactions of H_2 and higher hydrocarbon products, which is generally valid at low H_2 concentrations. A batch reactor model also assumes the system is homogeneous with uniform concentration and reactivity throughout the entire reactor volume, which is not true in the case of a plasma reactor. The plasma volume, or the active volume for reaction, is therefore significantly smaller compared to the reactor vessel, especially in our case. In order to account for this, a simple ideal dilution assumption was made where the reactor mixing timescale was assumed to be faster than the relevant reaction timescale. Further information regarding the derivation is in supporting information, S3. Equation 9 can be modified into the following:

$$\frac{d[CH_4]}{dt} = -\left(\frac{V_P}{V_R}\right)k_1[CH_4] = -k_{batch}[CH_4] \tag{10}$$

$$k_{batch} = \left(\frac{V_P}{V_R}\right)k_1 \tag{11}$$

$$\frac{[CH_4]}{[CH_4]_0} = e^{-k_{batch}t} \tag{12}$$

where V_P, V_R, $[CH_4]_0$, and k_{batch} are effective plasma volume, reactor volume, initial CH_4 concentration, and reaction rate constant measured in the batch reactor, respectively. In the mass transport-limited regime, the measured reaction rate constant can be a function of the Peclet number, which is the ratio of convective mass transport rate to diffusive mass transport rate inside of the plasma volume. Equation 11 shows that the reaction rate constant measured in the batch reactor is proportional to the true reaction rate constant with the proportionality constant being the volume fraction of plasma in the reactor. Experimental data show that CH_4 concentration decays exponentially with time, which follows a first-order reaction rate well. The rate constant can then be determined by linearizing Eq. 12 and fit to a semi–log dataset of normalized CH_4 concentration as shown in Fig. 4c.

To further validate Eq. 11, rate constants were measured at different electrode gaps with the same gas mixture. The reaction rate constant measured increased linearly with electrode gap length as demonstrated in Fig. 4d. This is expected if we assume the effective arc volume is a cylinder, which means the active volume increases linearly with the electrode gap (L_{gap}), Eq. 13. The effective cross-sectional area of the arc is estimated to be 0.44 mm^2 based on a series of images of the discharge, similar to Figs. 3a–d. The real rate constant (k_1) of CH_4 dissociation is estimated to be $9.44 \bullet 10^2$ s^{-1}, which corresponds to a gas temperature of 1990 K according to the rate parameters from Kevorkian et al. [22].

$$k_{batch} = \left(\frac{A_P}{V_R}k_1\right)L_{gap} \tag{13}$$

A_P is the effective cross-section area of the plasma arc.

Based on thermodynamic calculation (supporting information, section S4), methane dissociation from 1 to 10 bar pressure primarily yields solid carbon and H_2 at temperatures below 2300 K and C_2H_2 formation becomes more favorable above 2300 K. The calculation shows that no significant amount of C_2H_6 should form, which agrees with the lack of C_2H_6 species detected via mass spectrometry. The majority products of methane

conversion in low current arcs are C_2H_4, C_2H_2, amorphous carbon and H_2. The scanning electron micrograph of the carbon shows there is a distribution of carbon aggregates ranging from nanometers to microns, Fig. 5a. Product selectivities, as defined by Eqs. 4–6, are presented in Fig. 5b. C_2H_4 constitutes a significant portion of the product distribution in the experiment, which differs from the thermodynamic calculation. Further investigation into the temporal behavior of the product species shows that the product distribution of methane conversion has two distinct regimes. Initially, the selectivities for C_2H_4 and H_2 decrease, while the selectivities for C_2H_2 and carbon increase. As the reaction progresses, the product distribution reaches a state of pseudo-equilibrium as evidenced by the constant selectivities over time. Kado et al. examined the reaction pathway of methane conversion in a non-equilibrium pulsed spark discharge through isotope experiments [13]. They showed that C_2H_2 is likely formed from hydrogenation of atomic carbon or C_2, while C_2H_4 is simultaneously formed from hydrogenation of C_2H_2 and dehydrogenation of C_2H_6. On the other hand, it is demonstrated that thermal plasmas (e.g., arcs, some spark discharges, and microwave plasmas), follow Kassel's reaction scheme [23]. C_2H_6 is first formed from CH_3 radical recombination. Subsequently, C_2H_4, C_2H_2 and carbon are formed through a series of dehydrogenation steps. To understand the behavior of the product distribution observed in Fig. 5b, it is important to determine the significance of electron impact reactions and the reaction pathways in the low current AC arc plasma used in this study.

Effect of Different Inert Gases

A series of experiments with different Ar and He concentration ratios with a constant CH_4 partial pressure (0.4 bar) was conducted at 2 bar. Figure 6a shows the normalized concentration of CH_4 over time under different concentrations of Ar and He. The measured rate of CH_4 dissociation does not show any dependence on Ar and He ratio. This suggests that electron impact dissociation reactions may not play an important role in methane dissociation in low current AC arc discharges. Further investigation into the gas products shows that C_2H_4 selectivity is not affected by Ar concentration. However, the selectivity for C_2H_2 decreases from 52.5 to 40.6%, which is compensated by an increase in carbon selectivity, with increase in Ar concentration in the plasma as shown in Fig. 6b. The temperature in the plasma arc is estimated based on the blackbody emission from the soot particles using a reference blackbody source at 3100 K (Ocean Optics Cal-2000). The temperature increases

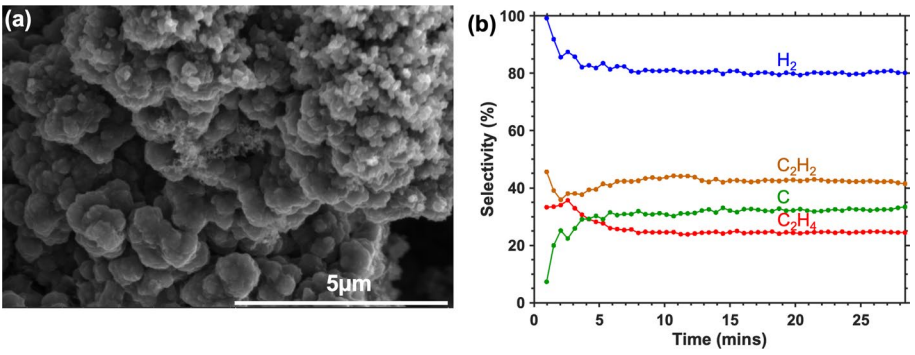

Fig. 5 **a** Scanning electron micrograph of amorphous carbon products from a methane plasma at 2 bar. **b** Progression of product selectivities during a 10% He/ 90% CH_4 discharge at 2 bar

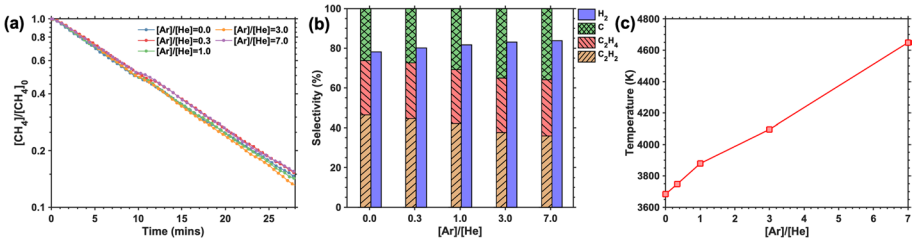

Fig. 6 Analyses of CH_4 conversion in 80% (Ar + He) and 20% CH_4 mixture discharges at 2 bar and 2.8 mm electrode gap length. **a** Decay of normalized CH_4 concentration with time during discharges at different Ar and He compositions. **b** Product selectivities corresponding to different Ar and He concentration ratios. **c** Gas temperature estimation from a rough fit of the soot particle blackbody emission, which shows an increase in temperature with Ar concentration

with increasing Ar concentration, shown in Fig. 6c. This possibly leads to an increase in the conversion of C_2H_2 to carbon, which corresponds with the increase in H_2 selectivity as well.

Impact of Hydrogen Partial Pressure on Methane Decomposition

To analyze the kinetics of methane dissociation and resultant product distribution, the influence of H_2 on methane dissociation was investigated through a series of experiments with different initial H_2 partial pressures ranging from 0.0 to 1.6 bar, corresponding to H_2 to CH_4 ratios of 0–8. The initial reactor pressure was held at 2 bar for all experimental conditions. The results show that the measured rate constant (k_{batch}) of CH_4 dissociation increases with H_2 partial pressure as evidenced by the increase in slope in Fig. 7a. This trend contrasts with experimental results shown in non-catalytic thermal CH_4 pyrolysis, which are typically conducted at temperatures between 950 and 1100°C [4, 5, 24]. H_2 partial pressure has been shown to impede the conversion rate of CH_4 due to the reverse reaction with H_2, which hydrocracks (hydro)carbon products back into CH_4.

In this study, the increase in rate constant results from the increase in H radical concentration from the additional H_2 species, which leads to an increase in the reaction rate of

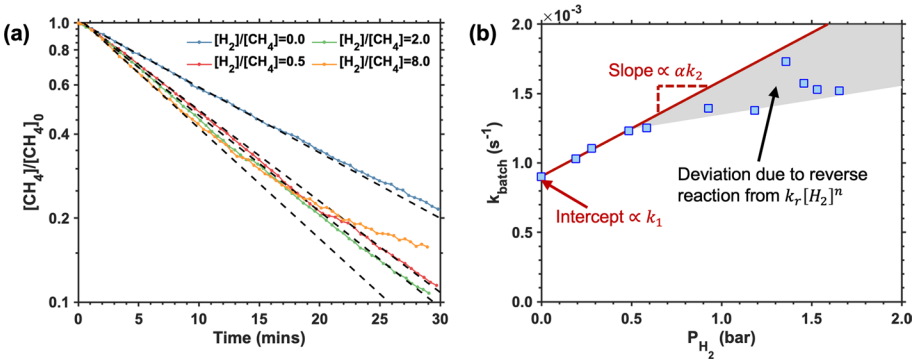

Fig. 7 **a** Normalized CH_4 concentration over time for different initial H_2 partial pressures at a total pressure of 2 bar and an electrode gap of 2.8 mm. The gas mixture contains 10% He and 90% CH_4 and H_2. **b** Dependence of reaction rate constant of CH_4 decomposition on H_2 partial pressure

H abstraction from CH_4, following Eq. 14. In addition, the rate constant for H abstraction reaction increases significantly with temperature, which means this radical dissociation reaction pathway becomes more prominent in a high temperature process. The rate of CH_4 dissociation can be modified to account for the contribution from the H abstraction reaction as shown in Eq. 15 (Derivation is shown in supporting information S5).

$$H + CH_4 \xrightarrow{k_2} CH_3 + H_2 \tag{14}$$

$$k_{batch} = \left(\frac{V_P}{V_R}\right)\left(k_1 + \alpha k_2 \left[H_2\right]_0\right) \tag{15}$$

α, k_2, $\left[H_2\right]_0$ are the degree of dissociation of H_2, the rate constant of Eq. 14, and the initial concentration of H_2. Equation 15 shows that the rate constant of CH_4 dissociation increases linearly with H_2 partial pressure. This relationship is in agreement with the experimental data up to a H_2 partial pressure of 0.6 bar, which corresponds to a H_2 to CH_4 molar ratio of 1.8, shown in Fig. 7b. As H_2 partial pressure increases further, the rate constant falls below the predicted values based on Eq. 15. This deviation from the model is attributed to an increase in the reverse reaction rate with H_2 concentration, which decreases the overall CH_4 dissociation rate. As shown in the case where the molar ratio of H_2 to CH_4 is 8, Fig. 7a, the kinetics of CH_4 dissociation deviates from the first-order rate law, which demonstrates significant contribution from the reverse reaction.

The presence of H_2 in a low current arc CH_4 plasma thus increases the reaction rate constant of CH_4 dissociation. A similar effect of H_2 on CH_4 conversion rate has been previously reported in a pulsed microwave plasma and pulsed DC discharges [25, 26]. This increase in the rate constant with H_2 is enabled by the H abstraction reaction, which is thermally activated. At high H_2 partial pressures, the benefits of this rate enhancement are unfortunately offset by H_2 hydrocracking reactions. This increase in the reverse reaction rate can therefore limit CH_4 conversion as the process becomes kinetically limited.

Figure 8 shows the selectivities of CH_4 conversion with different initial H_2 concentrations. In general, the selectivity for carbon decreases significantly because high H_2 concentration can hinder reaction channels and limit the formation of soot precursors from acetylene [27]. H_2 selectivity shows no clear trend with respect to the increase in H_2 concentration. The increase in H_2 concentration favors the formation of hydrogenated products as indicated by the increase in both C_2H_4 and C_2H_2 selectivities. However, when the molar ratio of H_2 to CH_4 increases above 1.0, the selectivity for C_2H_4 continues to increase, while C_2H_2 selectivity decreases.

Influence of Ethylene Conversion

To investigate the pseudo-equilibrium product selectivity at long reaction time observed in Fig. 5b, the reaction rate and products of C_2H_4 dissociation were examined under various H_2 partial pressures to simulate the environment during CH_4 conversion. The dissociation rate of C_2H_4 follows a first order reaction rate at low H_2 concentrations as shown in Fig. 9a. Similar to the case of CH_4 conversion, the rate constant of C_2H_4 dissociation increases with H_2 partial pressure due to the contribution from H abstraction reaction, shown in Eq. 16. As the molar ratio of H_2 to C_2H_4 increases above 1.0, the rate of C_2H_4 dissociation starts to deviate from a first-order rate law at longer reaction times, as shown by the nonlinear relationship between the semi-log of normalized C_2H_4 concentration and time. Furthermore,

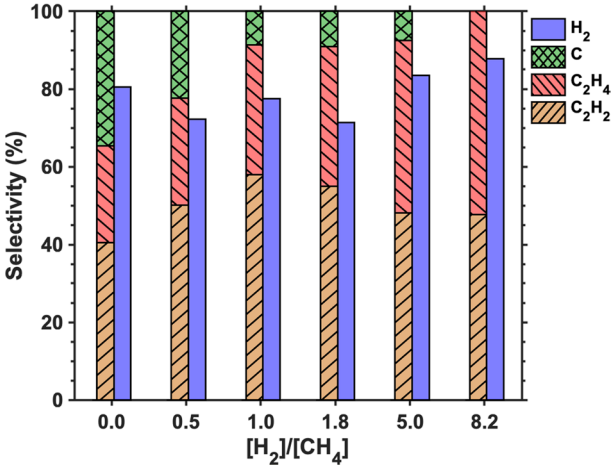

Fig. 8 Product selectivities at different initial H_2 partial pressures. The plasma was operated at a total pressure of 2 bar, an electrode gap of 2.8 mm, and with the H_2/CH_4 ratios shown

the adverse influence of high H_2 concentration due to hydrogenation and hydrocracking reactions in C_2H_4 dissociation appears to be more significant compared to CH_4 dissociation. As shown in the case of a molar ratio of H_2 to C_2H_4 of 8.0, the ethylene dissociation reaches a pseudo-equilibrium limit, where the conversion starts to plateau around 72%. In essence, the upper limit of C_2H_4 conversion is dependent on the H_2 concentration in the system.

$$H + C_2H_4 \rightarrow C_2H_3 + H_2 \tag{16}$$

Figure 9b shows the product selectivities of C_2H_4 conversion with different H_2 partial pressures. In pure C_2H_4 decomposition, amorphous carbon is the main product with a selectivity of 65%, which is higher compared to the selectivity of carbon obtained from CH_4 (~30%). As the H_2 partial pressure increases, the selectivity for carbon decreases, while C_2H_2 selectivity increases. This suggests that the presence of H_2 suppresses reaction channels that lead to conversion of acetylene to carbon and poly-cyclic aromatic hydrocarbons (PAHs). The conversion of C_2H_4 also produces CH_4, whose selectivity increases with H_2 partial pressure as well. This demonstrates that there is likely a hydrogen facilitated reaction pathway that converts C_2H_4 to CH_4.

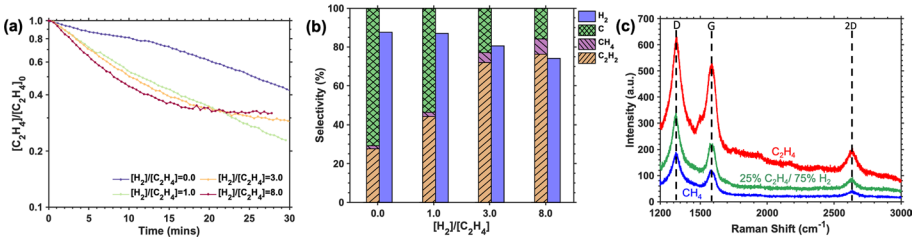

Fig. 9 **a** Normalized C_2H_4 concentration over time with different initial H_2 partial pressures at a total pressure of 2 bar and an electrode gap length of 2.8 mm **b** Product selectivities of C_2H_4 conversion under different initial H_2 partial pressures. **c** Raman spectra of carbon products from CH_4 and C_2H_4 conversion

The contents of the amorphous carbon product were analyzed via CH analyses shown in Table 1. The molar ratio of C–H in amorphous carbon converted from C_2H_4 is 12.1. As H_2 partial pressure increases, the carbon product becomes more hydrogenated, which is reflected in the decrease of C–H ratio to 9.73. For comparison, the C–H ratio of carbon converted from CH_4 is 6.31. This shows that carbon formed directly from C_2H_4 is less hydrogenated as compared to the carbon formed from CH_4. As might be expected, carbon products become more hydrogenated as H_2 concentration increases.

To further evaluate the carbon products, Raman analysis from 1200 to 3000 cm^{-1} were carried out (Fig. 9c). In general, there are three peaks at 1318, 1584 and 2633 cm^{-1}, which are the standard D, G, and 2D peaks, respectively. The G peak corresponds to in-plane vibration of carbon atoms within the graphite layers, while the presence of defects in graphitic carbon gives rise to the D and 2D peaks [28]. The D and G peak intensity ratio is a qualitative indicator of the degree of graphitization in the carbon products [29]. Table 1 shows D and G peak intensity ratios after subtracting the photoluminescence background using a polynomial fit. Increasing H_2 gas composition from 0 to 75% increases the D and G peak ratio of C_2H_4-produced carbon from 1.24 to 1.67. The increase in H_2 concentration leads to formation of less graphitic carbon, which agrees well with the increase in overall H content. Interestingly, the D and G peak ratio of CH_4 carbon is 1.67, which is similar to that of carbon obtained from a 25% C_2H_4 and 75% H_2 gas mixture. The latter further supports the aforementioned notion that carbon formation from CH_4 likely occurs through conversion of C_2H_4 and C_2H_2.

Impact of Pressure on Methane Decomposition

The effect of operating pressure on CH_4 decomposition was investigated from 0.5 to 3.1 bar. Figure 10a shows the concentration of CH_4 as a function of time at different pressures. The instantaneous rate of CH_4 dissociation (r_{CH_4}), as calculated by Eq. 17, increases from 0.02 to 0.11 $mol/m^3/s$ from an initial operating pressure of 0.5–3.0 bar. Further investigation shows that the rate constants (k_{batch}) initially decrease between the pressure range of 0.5 bar and 1.0 bar, but show no further dependence on pressure up to 3.0 bar, as demonstrated in Fig. 10b. As a result, the instantaneous rate of CH_4 decomposition increases almost linearly with pressure. To evaluate the efficacy of high-pressure operation, the specific energy requirement (SER) for CH_4 conversion was estimated based on the instantaneous rate and the corresponding plasma power input, Eq. 18. This approximation serves as the upper limit for SER calculation. The SER decreases monotonically from 672 to 365 kJ/mol_{CH_4} as the pressure increases from 0.5 bar to 3.0 bar as shown in Fig. 10c. Although the input power (P_{rms}) generally increases with operating pressure, the increase of CH_4 dissociation rate with pressure outweighs the increase in energy input.

Table 1 C–H ratio of 'amorphous' carbon from the plasma-based conversion of C_2H_4 and CH_4 and their corresponding ratio of D and G peak intensities from Raman spectroscopy

Gas Composition (%)				C:H Ratio	I_D/I_G
He	CH_4	C_2H_4	H_2		
10.0	90.0	–	–	6.31	1.67
10.0	–	22.5	67.5	9.73	1.67
10.0	–	90.0	–	12.1	1.24

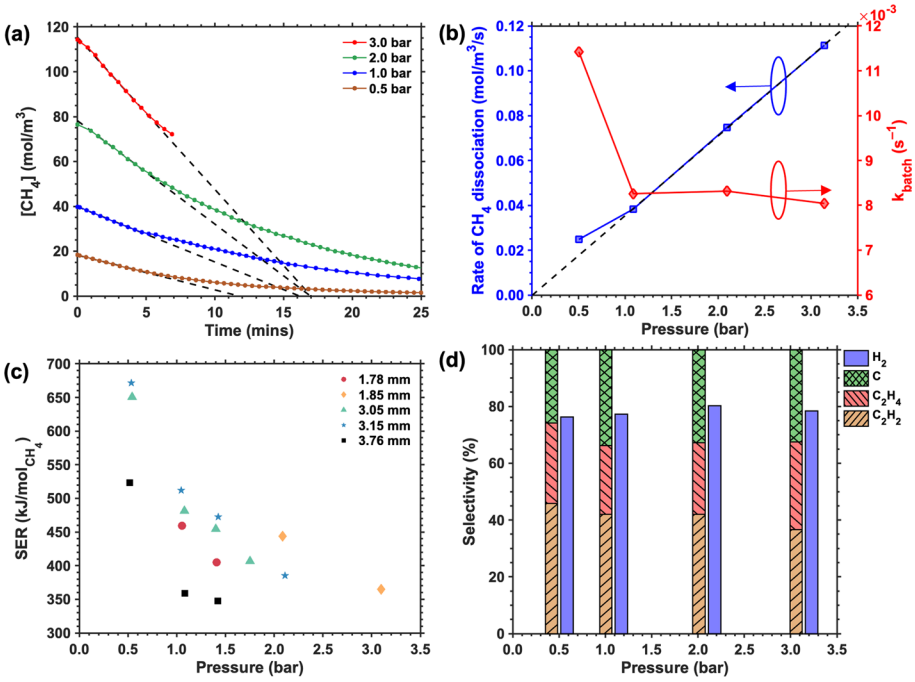

Fig. 10 **a** Concentration of CH_4 (based on total reactor volume) during the discharge as a function of time at different pressures with 2.8 mm electrode gap. The corresponding instantaneous rate of methane decomposition is estimated based on the initial CH_4 concentration and reaction rate constant, denoted by black dashed lines. **b** Dependence of instantaneous rate of CH_4 dissociation on reactor pressure. **c** Specific energy requirement (SER) for CH_4 conversion decreases with increasing pressure. The legend indicates the corresponding electrode gap lengths. **d** Product selectivities at different pressures with an electrode gap of 2.8 mm

This suggests that increasing operating pressure can serve as another important parameter in maximizing the energy efficiency of plasma conversion of CH_4.

$$-\frac{d[CH_4]}{dt}\Big|_{t=0} = k_1[CH_4]_0 \tag{17}$$

$$\text{SER} = \frac{\text{Average plasma input power}}{\text{instantaneous rate of } CH_4 \text{ dissociation}} = \frac{P_{avg}}{-\frac{d[CH_4]}{dt}\Big|_{t=0}} \tag{18}$$

The impact of operating pressure on the product distribution is shown in Fig. 10d. The H_2 selectivity ranges from 76 to 80% and shows no clear trend with pressure. For pressures from 0.5 to 1.0 bar, the selectivities of C_2H_4 and C_2H_2 slightly decrease, which is compensated by the increase in selectivity for carbon. As the pressure increases above 1.0 bar, the selectivity of C_2H_2 continues to decrease from 46 to 41%, while the selectivity of C_2H_4 increases from 24.2 to 30.8%. It is likely that hydrogenation reactions become more favorable at higher pressure, which leads to the increase in C_2H_4 products. The selectivity of

carbon does not show significant change with pressure from 1.0 to 3.0 bar. The corresponding Raman spectra of the carbon product do not show any significant difference as well, (Figure in supporting information S6).

Summary of Reaction Pathways in CH_4 Arc Plasma

The dominant reaction pathways corresponding to low current AC arc plasma conversion of CH_4 are demonstrated in Fig. 11, according to the results presented in the previous sections. Initially, CH_4 dissociates into methyl and hydrogen radicals through thermal dissociation channels. Once there is enough accumulation of H atoms, H abstraction reactions contribute significantly to CH_4 decomposition. The resultant CH_3 radicals can dissociate into CH_2 and CH, as supported by the presence of the CH emission line in Fig. 3f. In addition, CH_3 radicals can recombine to form ethane, which undergoes a series of dehydrogenation steps. The conversions of ethane to ethylene and ethylene to acetylene are facilitated by both dehydrogenation and H abstraction reactions. Similarly, acetylene can be converted into C_2 through H abstraction and dissociation reactions. Both acetylene and C_2 can then undergo a series of dimerization and dehydrogenation reactions to form carbon and polycyclic aromatic hydrocarbons (PAHs).

As the reaction progresses and H_2 concentration increases, hydrogenation reactions become more prominent, which creates a pathway for C_2H_2 and C_2H_4 regeneration as designated by the purple arrows in Fig. 11. This competition between dissociation and regeneration rates of C_2 products establishes a pseudo-equilibrium between the C_2 hydrocarbon products and H_2 in the system, which is consistent with the constant selectivities over time observed for C_2H_4 and C_2H_2 in Fig. 5b. Furthermore, high H_2 concentration enables reaction pathways for regenerating CH_4, which presumably occurs through some reaction channels involving C_2H_4. Although the current study does not provide enough information to determine this mechanism, the back conversion of C_2H_4 into CH_4 is likely facilitated by H atoms. C_2H_5 can be formed through H addition to C_2H_4, which can then dissociate into CH_3 radicals through a reaction with another H atom. CH_4 is then regenerated by recombination of a methyl radical with a hydrogen atom. An increase in pressure up to 3 bar does not appear to influence the dissociation pathway of methane, as suggested by the observed pressure-independent rate constant. However, hydrogenation reactions become more favorable at higher pressure.

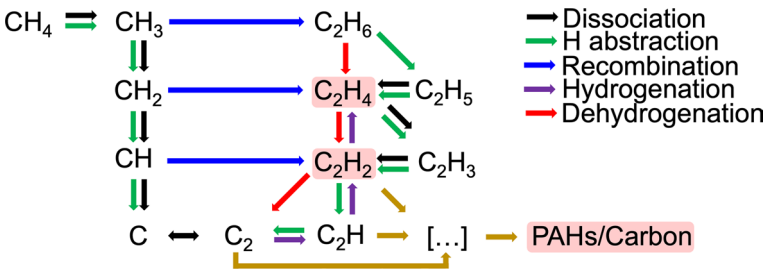

Fig. 11 Summary of probable reaction pathways of CH_4 dissociation in a low current AC arc discharge. PAHs denotes poly-cyclic aromatic hydrocarbons. The chemical species highlighted in red signify stable products. The gold arrow denotes unidentified reaction mechanisms (Color figure online)

Conclusion

To summarize, the kinetics and influence of pressure on CH_4 conversion in a low current AC arc discharge were examined. By developing a kinetics measurement methodology in a batch reactor, the dissociation rate of CH_4 under different pressure and gas conditions was evaluated. The results demonstrate there is little to no detrimental effect on the kinetics of CH_4 dissociation as the operating pressure increases up to 3.0 bar, which leads to a decrease in SER for CH_4 conversion from 672 to 365 kJ/mol_{CH4}. This finding emphasizes the potential of operating pressure as an important parameter in improving the efficiency of plasma conversion of CH_4 into H_2 and higher valued hydrocarbons.

Further investigation into the kinetics of CH_4 plasma reveals that CH_4 conversion occurs through thermal dissociation, and that H abstraction reactions play an important role in the dissociation of hydrocarbons in plasma conversion systems. Increase in H_2 concentration during the reaction leads to an increase in the activity of hydrogenation reactions, which impede the conversions of CH_4 and its C_2 hydrocarbon products. This leads to a pseudo-equilibrium between CH_4, H_2 and other gaseous products. As such, the presence of H_2 largely influence the kinetics of CH_4 dissociation, and the product distribution from the plasma. This provides valuable insights into plasma conversion of CH_4 to C_2 hydrocarbons and can inform the design of a more efficient plasma process that can be tuned towards higher selectivity for specific C_2 hydrocarbons while potentially minimizing the required energy input for their production.

The current study has mainly probed the influence of gas conditions on the kinetics of plasma conversion. Other plasma parameters such as input power, discharge gap, and different types of discharge, both thermal and non-thermal, can largely influence both the kinetics and the product distribution. The investigation of CH_4 conversion kinetics with these different parameters should be the subject of future studies.

Supplementary Information The online version contains supplementary material available at https://doi.org/10.1007/s11090-023-10416-w.

Author Contributions NL and MJG conceived and planned experiments. NL carried out experiments, analyzed data, and wrote the draft manuscript. YW assisted with experiments and supplemental information. MJG managed the project and edited the manuscript. All authors reviewed the final manuscript.

Funding This material was based upon work supported by the Robert G. Rinker Endowment for Chemical Engineering at UCSB, with auxiliary funding provided by C-Zero, Inc and the National Science Foundation Graduate Research Fellowship under Grant No. 2139319. The results presented made use of the MRL Shared Experimental Facilities of UCSB supported by the MRSEC program (NSF DMR 1720256), a member of the Materials Research Facilities Network (www.mrfn.org), as well as the UCSB Nanofabrication Facility, an open access laboratory.

Data availability All data generated or analyzed during this study are included in this published article and supporting information documents.

Declarations

Competing interests The authors declare no competing interests.

Ethical Approval Not applicable.

References

1. Parkinson B, Balcombe P, Speirs JF, Hawkes AD, Hellgardt K (2019) Levelized cost of CO_2 mitigation from hydrogen production routes. Energy Environ Sci 12(1):19–40. https://doi.org/10.1039/C8EE02079E
2. Patlolla SR, Katsu K, Sharafian A, Wei K, Herrera OE, Mérida W (2023) A review of methane pyrolysis technologies for hydrogen production. Renew Sustain Energy Rev 181:113323. https://doi.org/10.1016/j.rser.2023.113323
3. Ruscic B (2015) Active thermochemical tables: sequential bond dissociation enthalpies of methane, ethane, and methanol and the related thermochemistry. J Phys Chem A 119(28):7810–7837. https://doi.org/10.1021/acs.jpca.5b01346
4. Olsvik O, Rokstad OA, Holmen A (1995) Pyrolysis of methane in the presence of hydrogen. Chem Eng Technol 18(5):349–358. https://doi.org/10.1002/ceat.270180510
5. Holliday GC, Exell HC (1929) CXLI—the thermal decomposition of methane. Part I. Decomposition in silica bulbs. J Chem Soc (Resumed). https://doi.org/10.1039/JR9290001066
6. Li X-S, Zhu A-M, Wang K-J, Xu Y, Song Z-M (2004) Methane conversion to C_2 hydrocarbons and hydrogen in atmospheric non-thermal plasmas generated by different electric discharge techniques. Catal Today 98(4):617–624. https://doi.org/10.1016/j.cattod.2004.09.048
7. Kado S, Sekine Y, Nozaki T, Okazaki K (2004) Diagnosis of atmospheric pressure low temperature plasma and application to high efficient methane conversion. Catal Today 89(1–2):47–55. https://doi.org/10.1016/j.cattod.2003.11.036
8. Xu C, Tu X (2013) Plasma-assisted methane conversion in an atmospheric pressure dielectric barrier discharge reactor. J Energy Chem 22(3):420–425. https://doi.org/10.1016/S2095-4956(13)60055-8
9. Scapinello M, Delikonstantis E, Stefanidis GD (2018) Direct methane-to-ethylene conversion in a nanosecond pulsed discharge. Fuel 222:705–710. https://doi.org/10.1016/j.fuel.2018.03.017
10. Scapinello M, Delikonstantis E, Stefanidis GD (2019) A study on the reaction mechanism of non-oxidative methane coupling in a nanosecond pulsed discharge reactor using isotope analysis. Chem Eng J 360:64–74. https://doi.org/10.1016/j.cej.2018.11.161
11. Nozaki T, Muto N, Kado S, Okazaki K (2004) Dissociation of vibrationally excited methane on Ni catalyst. Catal Today 89(1–2):57–65. https://doi.org/10.1016/j.cattod.2003.11.040
12. Lotfalipour R, Ghorbanzadeh AM, Mahdian A (2014) Methane conversion by repetitive nanosecond pulsed plasma. J Phys D: Appl Phys 47(36):365201. https://doi.org/10.1088/0022-3727/47/36/365201
13. Kado S, Urasaki K, Sekine Y, Fujimoto K, Nozaki T, Okazaki K (2003) Reaction mechanism of methane activation using non-equilibrium pulsed discharge at room temperature. Fuel 82(18):2291–2297. https://doi.org/10.1016/S0016-2361(03)00163-7
14. Kreuznacht S, Purcel M, Böddeker S, Awakowicz P, Xia W, Muhler M, Böke M, von Keudell A (2023) Comparison of the performance of a microwave plasma torch and a gliding arc plasma for hydrogen production via methane pyrolysis. Plasma Processes Polym 20(1):2200132. https://doi.org/10.1002/ppap.202200132
15. Indarto A, Choi J, Lee H, Song H (2006) Effect of additive gases on methane conversion using gliding arc discharge. Energy 31(14):2986–2995. https://doi.org/10.1016/j.energy.2005.10.034
16. Fincke JR, Anderson RP, Hyde T, Detering BA, Wright R, Bewley RL, Haggard DC, Swank WD (2002) Plasma thermal conversion of methane to acetylene. Plasma Chem Plasma Process 22(1):105–136. https://doi.org/10.1023/A:1012944615974
17. Gautier M, Rohani V, Fulcheri L (2017) Direct decarbonization of methane by thermal plasma for the production of hydrogen and high value-added carbon black. Int J Hydrogen Energy 42(47):28140–28156. https://doi.org/10.1016/j.ijhydene.2017.09.021
18. Polak LS (1967) Low-temperature plasma in petroleum chemistry. Petrol Chem USSR 7(2):136–152. https://doi.org/10.1016/0031-6458(67)90032-9
19. Bilera IV, Lebedev YuA (2022) Plasma-chemical production of acetylene from hydrocarbons: history and current status (a review). Pet Chem 62(4):329–351. https://doi.org/10.1134/S0965544122010145
20. Fulcheri L, Rohani V-J, Wyse E, Hardman N, Dames E (2023) An energy-efficient plasma methane pyrolysis process for high yields of carbon black and hydrogen. Int J Hydrogen Energy 48(8):2920–2928. https://doi.org/10.1016/j.ijhydene.2022.10.144
21. Ohmori Y, Kitamori K, Shimozuma M, Tagashira H (1986) Boltzmann equation analysis of electron swarm behaviour in methane. J Phys D: Appl Phys 19(3):437–455. https://doi.org/10.1088/0022-3727/19/3/013
22. Kevorkian V, Heath CE, Boudart M (1960) The decomposition of methane in shock waves[1]. J Phys Chem 64(8):964–968. https://doi.org/10.1021/j100837a002

23. Kassel LS (1932) The thermal decomposition of methane[1]. J Am Chem Soc 54(10):3949–3961. https://doi.org/10.1021/ja01349a019
24. Palmer C, Gordon MJ, Metiu H, McFarland EW (2022) Influence of hydrocarbon feed additives on the high-temperature pyrolysis of methane in molten salt bubble column reactors. React Chem Eng 7(5):1199–1209. https://doi.org/10.1039/D1RE00517K
25. Heintze M, Magureanu M, Kettlitz M (2002) Mechanism of C_2 hydrocarbon formation from methane in a pulsed microwave plasma. J Appl Phys 92(12):7022–7031. https://doi.org/10.1063/1.1521518
26. Kado S, Sekine Y, Fujimoto K (1999) Direct synthesis of acetylene from methane by direct current pulse discharge. Chem Commun 24:2485–2486. https://doi.org/10.1039/a906914c
27. Slovetskii DI, Mankelevich YA, Slovetskii SD, Rakhimova TV (2002) Mathematical modeling of the plasma-chemical pyrolysis of methane. High Energy Chem 36:44–52
28. Ferrari AC, Basko DM (2013) Raman spectroscopy as a versatile tool for studying the properties of graphene. Nature Nanotech 8(4):235–246. https://doi.org/10.1038/nnano.2013.46
29. Ferrari AC, Robertson J (2000) Interpretation of Raman spectra of disordered and amorphous carbon. Phys Rev B 61(20):14095–14107. https://doi.org/10.1103/PhysRevB.61.14095